

Ultrafast and Highly Deformable Electromagnetic Hydrogel Actuators Assembled from Liquid Metal Gel Fiber

Daiki Tachibana, Koki Murakami, Takashi Kozaki, Ryosuke Matsuda, Yutaka Isoda, Fumika Nakamura, Yuji Isano, Kazuhide Ueno, Ohmi Fuchiwaki,* and Hiroki Ota*

Hydrogel actuators are ultrasoft and pliable but achieving high driving speeds with large deformation and fine local controllability is difficult because the driving force originates from the external air pressure or heat, and the base material is fragile. Herein, hydrogel actuators that allow high-speed driving and large deformation with high-frequency local controllability while maintaining softness are fabricated based on liquid metal gel fibers as electrodes by using microfluidic technology. The Lorentz force produced by an electric current and a magnet is used for actuation control. An ultrafast response of 260.5 mm s^{-1} with high-frequency controllability (6 Hz) and a large deformation of 172% with hydrogel actuation are observed. As proof of concept, moving stages, micromixers, and grippers exhibiting high speeds with high mechanical deformability while maintaining the inherent characteristics of hydrogel phases are demonstrated. Different hydrogels can be used with the proposed actuator architecture and fabrication scheme, enabling different functionalities.

1. Introduction

Soft actuators can perform bending and stretching motions in a manner similar to that by the human body. These characteristics can be used to create robots that closely replicate human behaviors. Their softness also allows for soft contact, and they

D. Tachibana, K. Murakami, T. Kozaki, R. Matsuda, F. Nakamura, Y. Isano, O. Fuchiwaki, H. Ota

Department of Mechanical Engineering
Yokohama National University

79-5, Tokiwadai, Hodogaya-ku, Yokohama, Kanagawa 240-8501, Japan
E-mail: fuchiwaki-ohmi-xk@ynu.ac.jp; ota-hiroki-xm@ynu.ac.jp

Y. Isoda, O. Fuchiwaki, H. Ota
Graduate School of System Integration
Yokohama National University

79-5, Tokiwadai, Hodogaya-ku, Yokohama, Kanagawa 240-8501, Japan

K. Ueno

Department of Chemistry and Life Science
Yokohama National University

79-5 Tokiwadai, Hodogaya-ku, Yokohama, Kanagawa 240-8501, Japan

 The ORCID identification number(s) for the author(s) of this article can be found under <https://doi.org/10.1002/aisy.202100212>.

© 2022 The Authors. Advanced Intelligent Systems published by Wiley-VCH GmbH. This is an open access article under the terms of the Creative Commons Attribution License, which permits use, distribution and reproduction in any medium, provided the original work is properly cited.

DOI: 10.1002/aisy.202100212

could thus replace conventional robots in fields such as minimally invasive medicine.^[1–5] Silicone rubber materials such as Ecoflex and polydimethyl siloxane (PDMS) are used most commonly as basal materials in soft actuators.^[6–8] Hydrogels can also be used to fabricate ultrasoft and ultralight actuators.^[9,10] A hydrogel is a polymer material with Young's modulus of 10^3 – 10^5 Pa and with properties intermediate between liquids and solids. Hydrogel actuators can perform smooth motions and fit easily into complex shapes. Therefore, they have found applications in biosensing systems, cell manipulation, and biometric motion.^[11–17]

In general, the motion of soft actuators is caused by various external stimuli such as heat, air pressure, electricity, or magnetic fields. Pneumatic actuators are widely

used in soft robotics and human assist devices because they can generate large forces.^[18–20] Dielectric elastomer actuators show excellent mechanical performance, although they require operating voltages of several thousand volts.^[21–23] Actuators have been fabricated by mixing liquid ethanol into silicone; these expand as ethanol vaporizes with increasing temperature.^[24,25] In case of hydrogel actuators, the actuators with heat, hydraulics, and magnetic fields as the operating principle have been proposed.^[26–28] In particular, although the local controllability is still low, a ball-type hydrogel actuator driven by light shows high speed rolling motion.^[29] Thus, it is still important to develop a hydrogel actuator that simultaneously affords a high reaction speed, large deformation, and fine local controllability (i.e., operability), with superior high-frequency response to replicate the behavior of living muscles.

Electromagnetism is an actuating principle that satisfies the three requirements mentioned above. Electromagnetically driven actuators using silicone rubber have been wired with a liquid metal inside the rubber material, and the Lorentz force generated by the electric and magnetic force realized high-speed drive with large deformation.^[30] Their movement can also be controlled using electricity. Liquid metal electrodes have a sufficiently low resistance to generate a Lorentz force with a low voltage. However, because hydrogel actuators comprise a hydrogel with an ultrasoft and superhydrophilic surface, it is difficult to wire them with a liquid metal on and/or inside the gel substrate.

Here, the present study proposes hydrogel actuators made of a gel and a liquid metal in which an electromagnetic force was used

to realize ultrafast drive and local controllability with superior high frequency. In biomedical and aquatic environments, electromagnetism-based gel actuators might lead to reduced safety. However, electromagnetic gel actuator is one of the best tools in terms of reaction speed and local control. By using electromagnetism in this study, we have provided a solution to a major problem of soft actuators. The electromagnetic force was driven through a liquid metal gel fiber embedded in a gel actuator by microfluidic technology. The coil shape of the gel fiber increased the stroke, thereby resulting in a large deformation of the gel simultaneously. As a result, an ultrafast actuator made of a gel and a liquid metal was realized, and its moving, bending, and expansion using electricity for control were demonstrated.

2. Results

2.1. Architecture and Fabrication of Liquid Metal Gel Fibers

Figure 1a shows the fabrication method of the liquid metal gel fiber used in this study. A gel fiber with a core-shell structure

was fabricated by dispensing a bilayer flow consisting of sodium alginate (AlgNa) and polyvinyl alcohol (PVA) solutions from a syringe needle. The inner PVA solution was replaced by a liquid metal to produce the liquid metal gel fiber. By applying an electric current to the liquid metal gel fiber in the hydrogel actuator placed within a magnetic field, a Lorentz force was generated to drive the gel actuator (Figure 1b). Three types of actuators that can perform translational and rotational movements as well as bending and expansion motions by controlling the current were demonstrated in this study (Figure 1c). The hydrogel actuator was fabricated by assembling the liquid metal gel fiber and an acrylamide gel as basal substrate.

As shown in Figure 1, the gel fiber comprises two layers: outer AlgNa gel and inner PVA solution. Figure 2a shows the relationship between the flow rates of the PVA solution and the AlgNa solution used to produce the gel fibers. When the PVA solution: AlgNa solution flow rate ratio was more than 1.00, the amount of PVA solution was too large and the AlgNa solution did not form a gel. Eventually, the solution mixture was dispensed from a needle. By contrast, when the flow rate ratio was less than

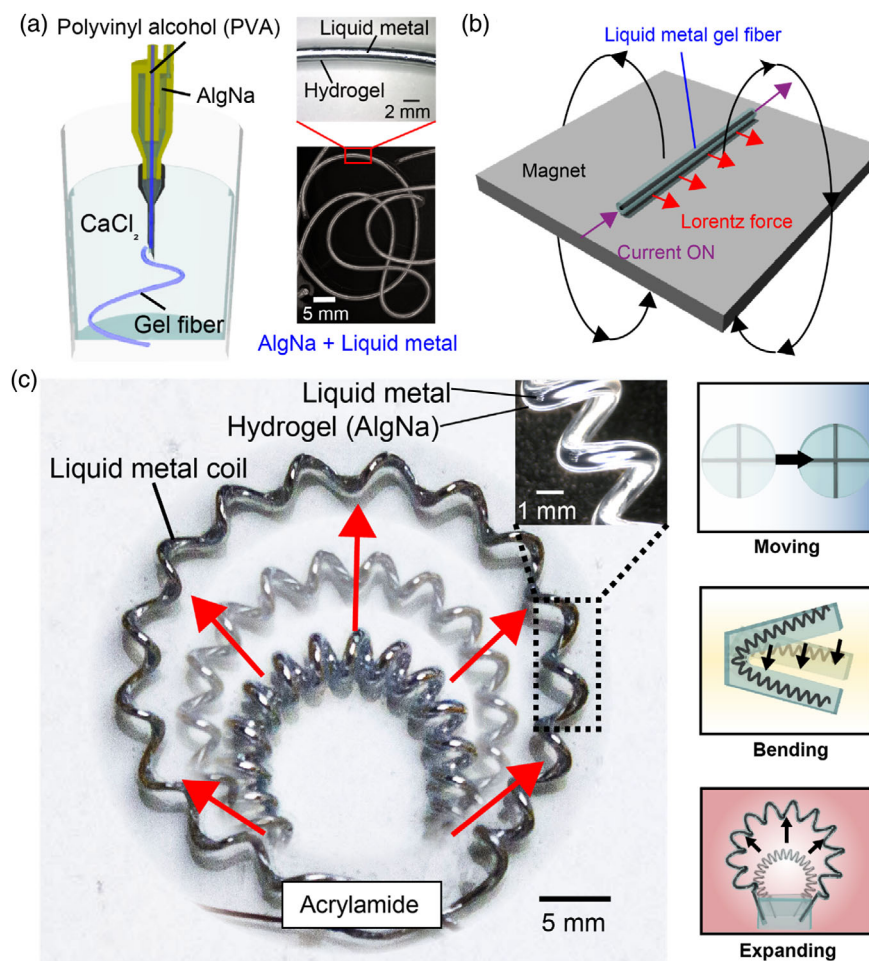


Figure 1. Schematic of ultrafast and highly deformable electromagnetic hydrogel actuators. a) Gel fiber fabrication method. Coaxially aligned nozzles and a needle were used to fabricate gel fibers with a core-shell structure. Then, liquid metal was injected into the core to produce liquid metal gel fibers. b) The actuator was driven by the Lorentz force generated by passing a current through the liquid metal gel fiber in a magnetic field. c) Gel actuator using liquid metal and magnetic force. Moving, bending, and expanding motions of hydrogel actuators by using electromagnetism and characteristics of structure.

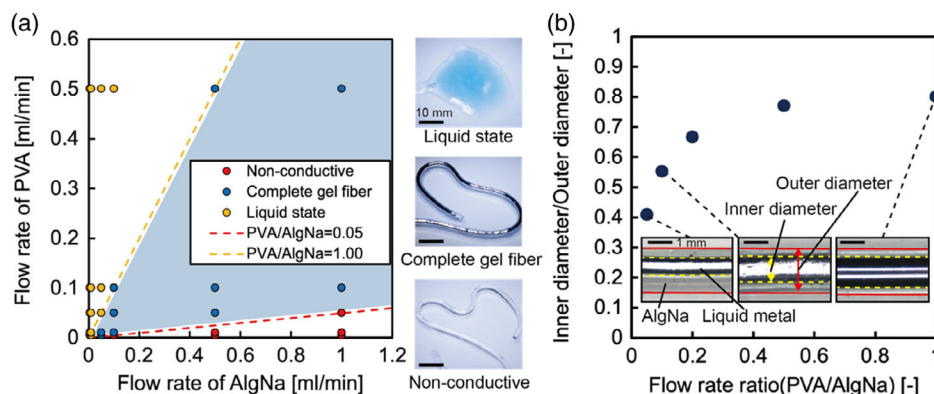


Figure 2. Design considerations for fabrication of liquid metal gel fiber. a) Relationship between flow rate of AlgNa solution and that of PVA solution. When the PVA:AlgNa flow rate ratio was more than 1.00, the amount of PVA solution was too large for the AlgNa solution to form a gel. b) Relationship between PVA solution:AlgNa solution flow rate ratio and inner diameter:outer diameter ratio of the gel. The inner diameter:outer diameter ratio increased as a function of the flow rate ratio. The upper limit of the inner diameter:outer diameter ratio was 0.8.

0.05, the flow rate of the aqueous AlgNa solution was too high to form a two-layer fiber structure with the PVA solution, resulting in a single-layer gel fiber into which the liquid metal could not be injected. Figure 2b shows the PVA solution:AlgNa solution flow rate ratio and the inner diameter:outer diameter ratio of the fabricated gel fiber. The inner diameter part was later replaced by liquid metal from PVA. The inner diameter indicates the PVA portion, and the outer diameter indicates the “PVA + AlgNa” portion. With increasing “PVA flow rate/AlgNa flow rate,” the PVA flow rate (inner diameter) relative to the overall flow rate increases as well. Therefore, the inner diameter:outer diameter ratio increased as the PVA solution:AlgNa solution flow rate ratio increased because the flow rate ratio of the PVA solution increased.

2.2. XY-Axis Moving Stage

To investigate the speed that can be generated in principle, we developed a simple structured XY-axis moving stage. **Figure 3a** shows a photograph of the XY-axis moving stage. Two gel fibers were wired in a cross shape inside the acrylamide gel. The direction of the force under both translational and rotational movements was calculated using the finite element analysis software COMSOL ver. 5.6 (**Figure 3b**). **Figure 3b(i)** shows that placing a magnet under the gel actuator and controlling the current flow enables omnidirectional movement of the actuator.

Furthermore, **Figure 3b(ii)** shows that arranging two magnets inside out produces symmetric but opposite forces at their boundary, thereby enabling rotational movement of the actuator.

Figure 3c shows the relationship between the time and the amount of movement when a current is applied to the XY-axis moving stage. The current was varied from 1 to 3 A. The amount of movement increased with the current. A mechanics model was developed, and the theoretical values are plotted in **Figure 3c** (Supporting text 1 and **Figure S1**, Supporting Information).

Figure 3d shows the results of controlling the movement direction of the actuator. Assuming that the current flowing along the X- and Y-axes of the device is A_X and A_Y ,

respectively, the theoretical angle from the X-axis is obtained based on the ratio of the currents, as given in Table S1, Supporting Information, (Supporting text 2 and **Figure S2**, Supporting Information). The average error between the theoretical and the experimental values was 3° , and the average of the standard deviation was 5° .

Figure 3e shows the trajectory when the actuator was moved in three directions. When a current was passed through the actuator in the positive Y-axis direction, negative X-axis direction, and both positive Y-axis and negative X-axis directions, the stage moved in the right, upward, and upward right directions, respectively. When the currents flowed in both electrodes, the stage moved upward at an angle of approximately 45° .

Figure 3f shows the situation when the actuator was rotated clockwise and counterclockwise. The fiber positions along the X- and Y-axes of the actuator were swapped after the 90° rotation of the hydrogel actuator. The actuator was rotated 180° by controlling the current flow so that the current flowed in the fiber along the X-axis direction at any point.

Figure 3g shows the relationship between the time and the rotation angle of the XY-axis moving stage. The amount of movement was plotted every $1/60$ s after the current was applied. Both theoretical and experimental rotation speeds increased with the applied current (Supporting text 3 and **Figure S3**, Supporting Information).

Figure 3h shows the stage orbit when the square orbit was controlled. The stage was controlled by changing the current direction with a control circuit. **Figure 3d** shows that an error of a few degrees existed in each direction. However, the orbit of the actuators could be controlled automatically following the control circuit.

2.3. Properties of Gel Fiber

Figure 4a shows the COMSOL simulation results and the experimental results when the straight-shaped fiber was deformed by Lorentz forces, and **Figure 4b** shows the corresponding results when the coil-shaped fiber was deformed. These figures show that in both the simulation and the experimental results, the

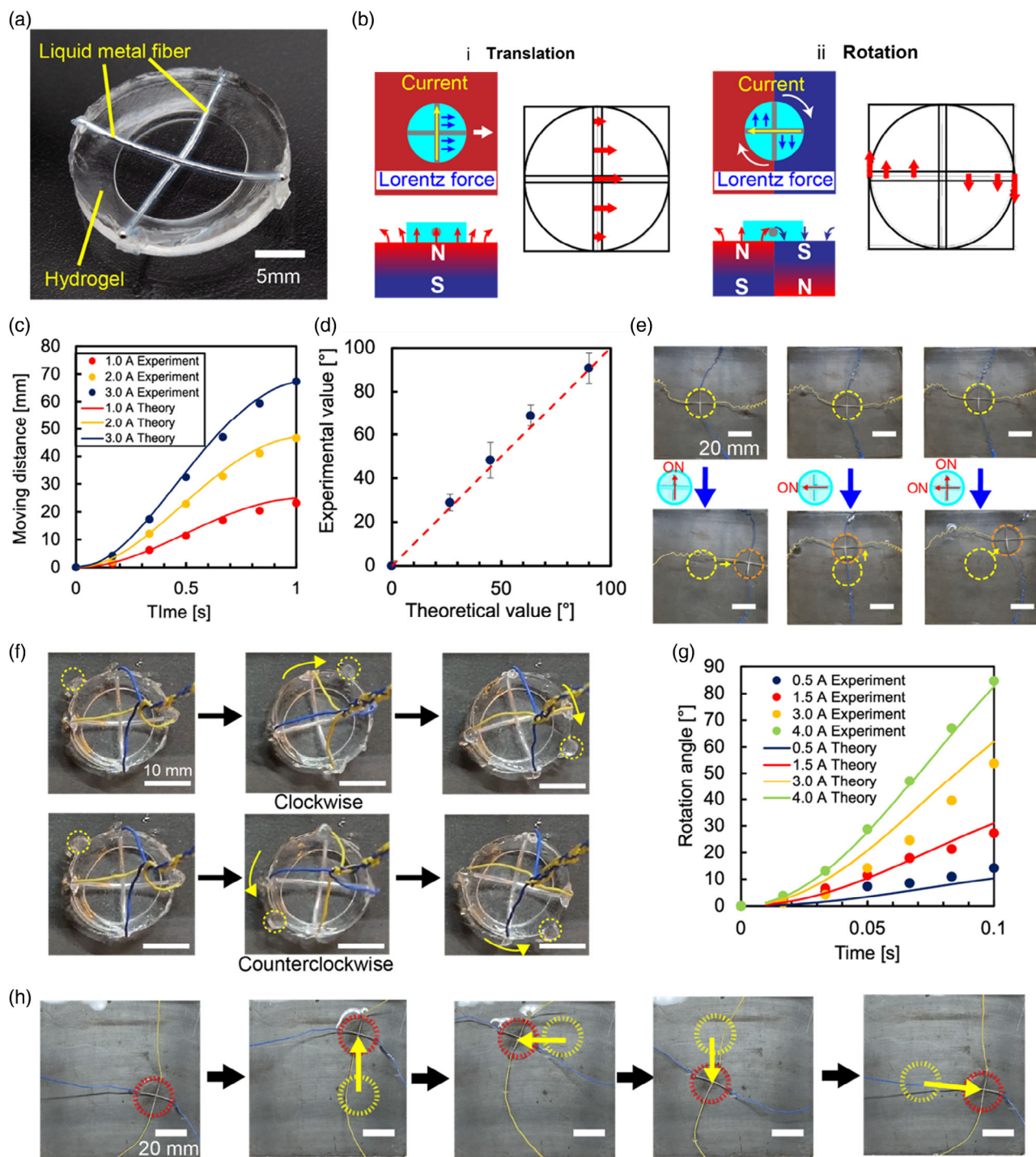


Figure 3. XY-axis moving and rotating stage using liquid metal gel fiber. a) Photograph of XY-axis moving and rotating stages. b) COMSOL simulations of Lorentz force when using one magnet and two aligned magnets. Forces for translation and rotation were determined by the relationship of the directions of the current and magnetic field. c) Relationship between time and moving distance of XY-axis moving stage. Current was varied from 1.0 to 3.0 A. Owing to the drag force of water, tension of copper wire, and change in magnetic flux density, both theoretical and experimental velocities were dampened. d) Relationship between experimental and theoretical values by controlling ratio of current flow in two electrodes. The movement direction in the XY plane could be controlled by the ratio of currents along each axis. e) Actual movements of hydrogel actuator in 0°, 90°, and 45° directions. f) Actual rotations of hydrogel actuator in clockwise and counterclockwise directions from -180° to 180° using two arranged magnets. g) Relationship between time and rotation angle of XY-axis moving stage. Current was varied from 0.5 to 4.0 A. h) Programmed square orbit control of hydrogel actuator performed by periodically changing the time and direction in which the current was passed through the two fibers.

amount of deformation in the coil-shaped fiber was larger than that in the straight-shaped one. The deformation directions in the straight- and coil-shaped hydrogel actuators were controlled by the current flow. For the straight-shaped fiber, the applied Lorentz forces follow Fleming's left-hand rule, as shown in Figure S4a, Supporting Information. By contrast, for the coil-shaped fiber, the resultant force derived from the Lorentz forces in the direction perpendicular to the main axis was applied, as shown in Figure S4b, Supporting Information. The resultant forces in the direction of the main axis canceled each other out.

Figure 4c shows that the coil-shaped fiber was deformed by around two times as much as the straight-shaped fiber with a 0.5 T neodymium magnet. The deformation of both types of

fibers decreased with a 0.1 T ferrite magnet, as shown in Figure S5, Supporting Information. The amount of deformation depended on the strength of the magnet.

Figure 4d shows the voltage and amplitude waveforms when a sinusoidal voltage was applied at a frequency of 1.0 Hz to vibrate the fiber. A phase delay of 1/30 to 1/10 s existed with respect to the input waveform.

Similarly, Figure 4e shows the amplitude response curve when a sine wave was applied. The frequency at the time of maximum amplitude, shown on the horizontal axis of Figure 4e, is normalized as 1. The horizontal axis in Figure S6, Supporting Information, shows the absolute value of the frequency. From Figure 4e and S6, Supporting Information, the resonance

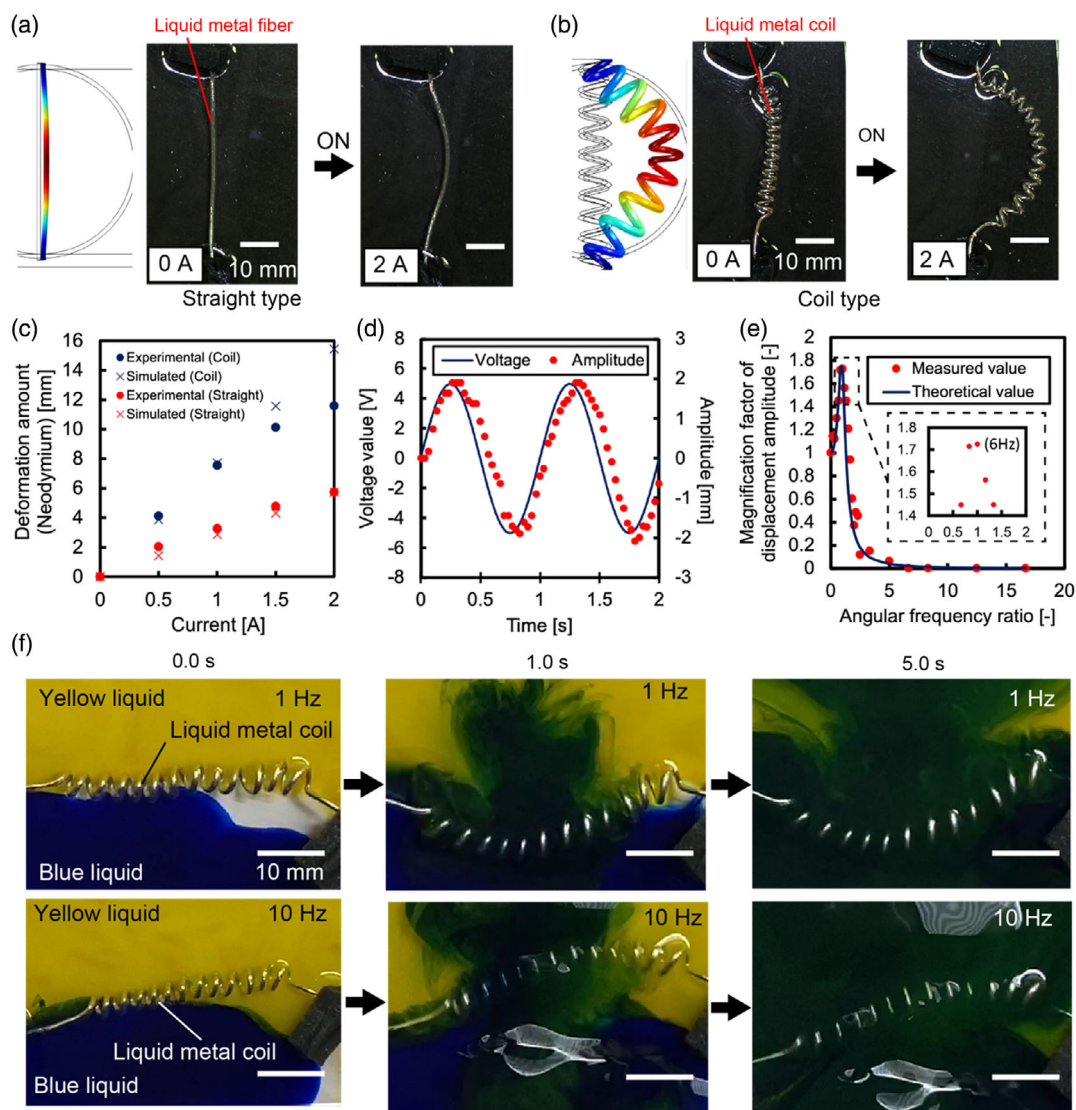


Figure 4. Physical and electromagnetic properties of straight- and coil-type liquid metal gel fiber. a) Deformation of straight-shaped gel fiber in experiment and COMSOL simulation. b) Deformation of coil-shaped gel fiber in experiment and COMSOL simulation. c) Relationship between deformation amount of gel fibers with neodymium magnet and current flow in liquid metal gel fiber. Deformation for both fiber types increased with the current. d) Voltage and amplitude waveforms when a sinusoidal voltage was applied at a frequency of 1.0 Hz to vibrate the fiber. e) Frequency response curve when a sine wave was applied. f) Demonstration of mixing of two inks by coil-shaped gel fiber when voltage was applied at 1 and 10 Hz.

frequency was 37.7 rad s^{-1} (6.0 Hz) and the maximum amplitude magnification was 1.73. Figure 4f shows the amplitude at frequencies of 1.0 and 10.0 Hz. Yellow and blue inks were mixed using the coil-shaped fibers with vibrations at 1 and 10 Hz (Figure 4f, Movie S1, Supporting Information). At 10.0 Hz, the green region became larger, indicating that the two inks were well mixed. Young's modulus of the gel fiber could be altered by varying the AlgNa(aq) concentration, as shown in Figure S7, Supporting Information.

2.4. Bending and Ring Grippers

As shown in Figure 5a, bending grippers were fabricated using both the straight- and the coil-shaped fibers. For both grippers, when a current was applied, a force was generated in the direction in which the gripper closed (Movie S2, Supporting Information). Figure 5b shows the relationship between the current applied to the bending gripper and the angle of the gripping part. For both grippers, the angle decreased with increasing

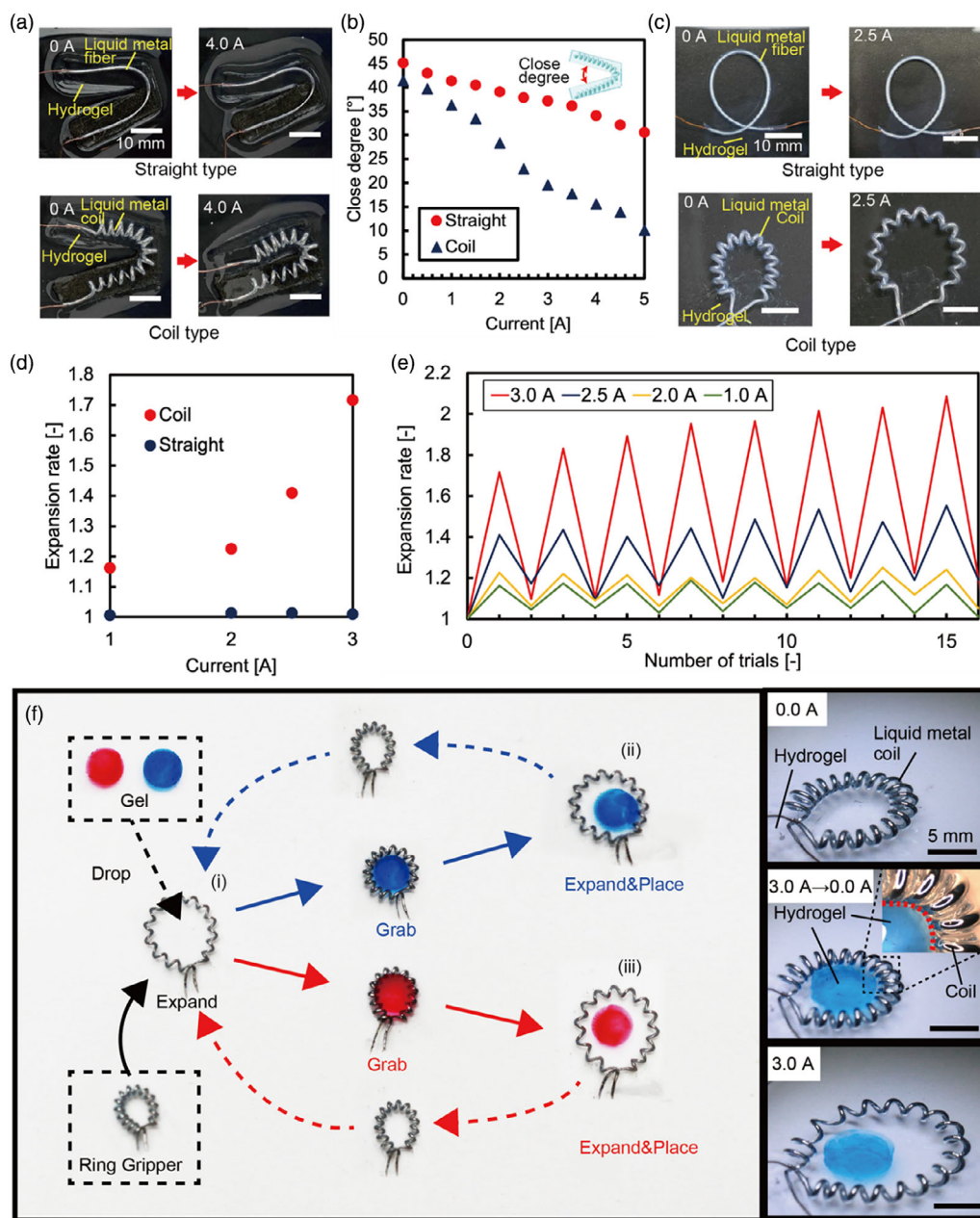


Figure 5. Hydrogel bending and expansion-shrinkage grippers using liquid metal. a) Photographs of bending grippers with straight- and coil-shaped gel fiber. b) Relationship between current and angles of grippers using straight- and coil-type fibers. Grippers closed with the applied current. Bending gripper using coil-type fiber closed more efficiently. c) Photographs of ring grippers with straight- and coil-shaped gel fiber. d) Expansion rates of ring grippers with straight- and coil-shaped gel fibers. Gripper expanded with increasing current. e) Repeatability test (up to 15 cycles) of ring gripper with coil-type fiber for currents of 1.0–3.0 A. f) Demonstration of grabbing, moving, and releasing gel objects using ring gripper.

current because of the Lorentz forces. The gripper with coil-shaped fibers closed more than did that with the straight-shaped fiber. This was because the straight fiber was deformed by the expansion and contraction of the material itself, whereas the coil fiber was deformed by the change in pitch (Figure S8, Supporting Information).

Figure 5c and Movie S3, Supporting Information, show the expansion and contraction of the ring gripper. Figure 5d shows the relationship between the current applied to the ring gripper and the enlargement ratio. The enlargement ratio R_x was calculated as

$$R_x = \frac{d_x}{d_0} \quad (1)$$

Here, d_x and d_0 are the diameters of the gripper after and before the current was applied, respectively. The coil-shaped gripper expanded with increasing current, whereas the straight-shaped gripper did not expand at all regardless of the current.

Figure 5e and S9, Supporting Information, show a repeatability test of the functionality of the ring gripper. The magnitude of deformation depended on the applied current, as shown in Figure 5d. When a current of 1 A was applied, the deformability was maintained over more than 100 cycles, as shown in Figure S9, Supporting Information. However, the hydrogel material deformed plastically upon repeating large deformations under a high applied current exceeding 2 A.

Figure 5f and Movie S4, Supporting Information, show that the ultrasoft ring gripper could be used to perform hydrogel block transportation. Neodymium magnets were placed at three locations so that expansion by current flow could be performed at those locations. First, the gripper grasped a blue hydrogel object at location (i) and then moved and released it at location (ii). Next, the same gripper grasped a red hydrogel object at location (i) and then moved and released it at location (iii). To show that the same gripper can be used for multiple operations, the gel of the object was divided into red and blue colors. The gripper could successfully grasp and move the soft, slippery hydrogel material multiple times.

3. Discussion

As shown in Figure 3b, the XY-axis moving stage can be moved and rotated by generating forces in the translation and rotation directions. In general, the direction of magnetic force lines became perpendicular to the magnet toward the center. Therefore, a stronger magnetic force can be generated near the center. COMSOL numerical calculation results showed that a larger Lorentz force was generated in the central part of the device during movement. Further, the Lorentz force increased toward the outside of the actuator during rotation because two magnets were arranged.

As shown in Figure 3c, the movement of the XY-axis moving stage increased with respect to the current. A dynamics model was set up as shown in Supporting text 1 and Figure S1, Supporting Information. The theoretical and experimental values

were compared. The equation of motion for the stage moving through water is expressed as follows

$$m\ddot{x} = F_g - F_D - F_k \quad (2)$$

Here, F_g is the Lorentz force; F_D is the drag force of water acting on the stage; and F_k is the damping force due to changes in tension and magnetic flux density. The expression of each parameter can be substituted into this equation to obtain

$$m\ddot{x} = BIL - C_D A \cdot \frac{1}{2} \rho v^2 - kx \quad (3)$$

The solution of this differential equation was obtained by the fourth-order Runge–Kutta method and plotted as a theoretical value in Figure 3c. The Lorentz force was generated in the movement direction. The acceleration decreased with time because the drag force of water and damping force due to tension occurred in the direction opposite to the movement direction. Therefore, as shown in Figure 3c, because the drag force was proportional to the square of the velocity, the acceleration decreased as the velocity increased and converged to the terminal velocity.

As shown in Figure 3d, when the stage was moving in the upper right 45° direction, the error was particularly large, and the standard deviation was approximately $\pm 8^\circ$. When it was moving in an oblique direction, current had to be applied to the two axes simultaneously. If even a slight deviation occurred, a rotational movement would occur owing to the force imbalance. Therefore, the error was considered to become larger than in the other cases.

The theoretical values of the rotation motion were also calculated from the equations of motion (Supporting text 3 and Figure S3, Supporting Information). For rotation motion, the forces generated on the stage were the torques, N_g , N_k and N_D due to the Lorentz force, tension of the copper wire, and viscous resistance of air, respectively. Thus, the equation of motion was given as

$$J\ddot{\theta} = N_g - N_D - N_k \quad (4)$$

If the torque due to the viscosity force, N_D is omitted, θ can be given as

$$\theta = \frac{BIR}{2k} \left(-\cos 2\sqrt{\frac{2k}{mR}}t + 1 \right) \quad (5)$$

The rotational speed at each time was calculated by substituting each parameter into Equation (5). For 0–0.03 s, the rotational angle increased exponentially with time. After 0.03 s, the slope and speed became constant. As the amount of rotation increased, the effect of the tension of the copper wire increased. The force might act in a direction that prevents rotation, resulting in a decrease in speed.

The XY-axis moving stage was driven by a Lorentz force by applying a current to the gel and an external magnetic force. Actuators can be driven by the magnetic gel and an external magnet or by the magnetic gel and an external coil.^[31,32] When using a magnetic gel and external magnet, the degree of freedom of movement was limited because the magnetic gel has only one

direction of magnetic force. When using an external coil, the nonuniform direction of the magnetic field made control difficult. In this study, the movement of the hydrogel actuator was controlled by the ratio of the current flows in two electrodes. As a result, the degree of freedom of the hydrogel movement could be improved and controlled easily. Thus, the direction of movement and rotation can be controlled and the speed can be adjusted instantaneously according to the current value. It is also possible to repeat the programmed motion as shown in Figure 3h. In this respect, the actuator is excellent for local control. However, our device required a large current for actuation. Therefore, a future study will aim to decrease the current required to generate the force.

We modeled the actuator by the second order lag element (Supporting text 4 and Figure S10, Supporting Information). We defined M_d as the magnification factor of the displacement amplitude, which is given by

$$M_d = \frac{1}{\sqrt{\left\{1 - \left(\frac{\omega}{\omega_n}\right)^2\right\}^2 + \left(2\zeta \frac{\omega}{\omega_n}\right)^2}} \quad (6)$$

In a second-order lag element, the natural angular frequency, ω_n and the damped natural angular frequency, ω_d are as follows

$$\omega_n = \sqrt{\frac{k}{m}} \quad (7)$$

$$\omega_d = \omega_n \sqrt{1 - \zeta^2} \quad (8)$$

where ζ and m are the damping ratio and weight, respectively. When ω is equivalent to, ω_d M_d becomes maximum. We define the maximum M_d as M_{dmax} . Here, ζ is represented as a function of, M_{dmax} which is given from Equation (6) and Equation (8) as follows

$$\zeta = \sqrt{\frac{2}{3} + \sqrt{\frac{4}{9} - \frac{1}{3M_{dmax}^2}}} \quad (9)$$

By substituting the experimentally obtained M_{dmax} of 1.73 in Equation (9), ζ is estimated to be 0.30. As shown in Figure 4e, the theoretical curve was obtained for a ζ value of 0.30. In this case, $\zeta < 1$ and therefore, the damping state is classified as insufficient damping, and the vibrations can be expected to occur even when free vibration is performed. The weight of the actuator m , which was 0.52 g, was measured using an electric balance. From Equation (7) and (8), we estimated the equivalent linear spring constant k of 0.81 N m⁻¹ using the following expression

$$k = \frac{m\omega_d^2}{1 - \zeta^2} \quad (10)$$

As shown in Figure 4e, the damping ratio was 0.30; this was classified as insufficient damping. The coil comprising the gel fiber vibrated even under free vibration, and the gel fiber was elastic. The damping ratio of the rubber material was approximately 0–0.3.^[33] The damping ratio of the gel fiber was almost the same. Therefore, the coil-type gel fiber was ultrasoft and had the elasticity of rubber. When using this fiber in the actuator,

its elasticity can be utilized as a driving force; this makes it a highly versatile material.

As shown in Figure S7, Supporting Information, Young's modulus decreased with the AlgNa concentration. Gel fibers could be produced with AlgNa concentrations of 3–6%. At concentrations below 3%, the gel became liquid and did not harden sufficiently. Further, at concentrations exceeding 6%, the viscosity of the AlgNa solution became too high, making stable coil formation difficult. Young's modulus of the hydrogel was related to the magnitude of deformation (expansion). Therefore, depending on the application, the concentration must be adjusted when forming coils.

The maximum generative force F_{max} was simulated by COMSOL in Figure 4b as 0.010 N under a current I of 2 A, length L of 30 mm, and a neodymium magnetic plate with 0.5 T of surface magnetic flux density. We also roughly estimated F_{max} by the principal formula of Lorentz force given by

$$F_{max} \approx I \cdot B_a \cdot L = 0.011 \text{ N} \quad (11)$$

The result based on the formula was almost the same as the one obtained using COMSOL. Here, B_a is the magnetic flux density, where the center of the actuator was arranged. B_a was experimentally obtained as 0.176 T using a gauss meter. **Table 1** shows the quantitative evaluation of the fabricated actuator when we modeled it as the second delay system.

The ratio of the generative force to the weight of the actuator was also an important factor. The generative force of the proposed actuator was roughly twice that of the weight of the actuator (i.e., the generative force was 0.01 N (1 gw) with the weight of the moving part being 0.5 g). We plan to discuss the improvement in the ratio of the generative force including multiple connections of actuators in future studies, and also discuss the insulation coating and the improvement in durability.

As shown in Figure 5b and S8, Supporting Information, the coil-type fiber could bend by 15°–20° more compared to the straight-type fiber. Based on this result, the five pitches in the deformed part were related to the bending in the coil shape. In other words, one pitch in the coil might generate a bending effect of approximately 3°–4°. By realizing a structure with more pitches of bending-related parts, fast and more flexible bending could be achieved.

As shown in Figure 5c–e, under a Lorentz force, the ring gripper could perform a significantly large expansion owing to its coil shape. Then, it returned to its original shape owing to the elasticity of the fiber. Therefore, the force required to grip the object depended on Young's modulus of the ring gripper.

Soft actuators with a fast deformation velocity and large expansion coefficient while maintaining a high-frequency local controllability were fabricated in this study. **Figure 6** shows the deformation speed of the device from its original shape with fine local controllability. Soft actuators mainly use heat, air pressure, light, and electric current as driving principles. In terms of actuators that use heat as the driving principle, the drive speed of the actuator becomes significantly slower because ethanol requires considerable time to evaporate and deform the substrate with increasing temperature.^[24,25] Actuators that use air pressure as the driving principle have been fabricated using silicone rubber and a robust hydrogel. These can deform through expansion,

Table 1. Quantitative evaluation of the coil-type gel fiber actuator when modeled as a second-order lag element.

Physical quantity	Symbol	Value	Unit	Obtaining method
Weight	m	0.52	g	Measured by an electric balance
Damped natural angular frequency	ω_d	37.7	rad s ⁻¹	Obtained from Figure S6, Supporting Information
Damped natural frequency	f_d	6.0	Hz	Obtained from Figure S6, Supporting Information
Damping ratio	ζ	0.30		Calculated from Equation (9)
Quality factor	Q	1.67		Calculated from approximation of $1/(2\zeta)$
Maximum generative force ($I = 2\text{ A}$)	F_{max}	0.010	N	Simulation result using COMSOL
Linear spring constant	k	0.81	N m ⁻¹	Calculated from Equation (10)

contraction, and bending upon injecting air.^[18–20] A pneumatically actuated soft actuator made of a hydrogel has a velocity of approximately 0.5–1 mm s⁻¹. This is lower than the velocity achieved in our study.^[34,35] However, as a hydrogel actuator, it can generate enough force and is robust. In actuators that use light as the driving principle, deformation was produced through the photoisomerization of the material. An actuator was fabricated by combining a light-responsive liquid crystal network (LCN) film with a silicone rubber material such as PDMS.^[36] Although light irradiation can be performed at high speed, the deformation speed was comparable to that of pneumatic actuators because the driving speed was determined by the time required for the structural change of the LCN. In addition, the ball-type hydrogel actuator driven by light showed rolling motion at 1.6 m s⁻¹.^[29] However, it might be difficult to achieve fine local control and to add additional functionality other than rolling and jumping such as grasping. In Figure 6, the ball-type hydrogel actuator was excluded. From the deformation speed results in Figure 6, when using electricity as the driving principle, the actuator can be driven at high speed when using a material as hard as silicone rubber. For achieving high-speed drive with electricity, a material with the hardness of silicone rubber has been used often as the substrate material of the actuator.^[30,37–40] In particular, as in the present study, ultrafast drive-in hydrogel actuators can

be realized when using electric current and neodymium magnets.^[29]

Conventional gel actuators basically operate by using the swelling of the gel. For thermoresponsive gels such as PNIPAM that swell because of heat, the amount of expansion (i.e., expansion rate) relative to contraction is approximately 30–40%.^[26] In the case of connecting electrodes and when using the movement of ions inside the gel, the swelling inside the gel changed with ion movements, causing bending deformation. The basic operation of the actuator was bending motion. The bending force was generated by an expansion force by fixing a part of the gel or a bilayered structure. In this case, the amount of expansion was approximately 20% at most.^[41,42] Some gel actuators can perform bending motion through hydrodynamic pressure produced by injecting water into the gel. However, although such actuators can bend and deform at high speed, they can hardly expand or contract.^[27] Our proposed electromagnetic gel actuator with a ring gripper based on a coil-type gel fiber enabled a large expansion motion by using the expanding/contracting structure of the coil. As shown in Figure 5d, the developed ring gripper achieved a magnification ratio of 1.72 times at a current of 3 A. This magnification was equivalent to that of a soft actuator made of a rubber material. In conclusion, a gel actuator that can deform sufficiently at high speed was developed successfully in this study.

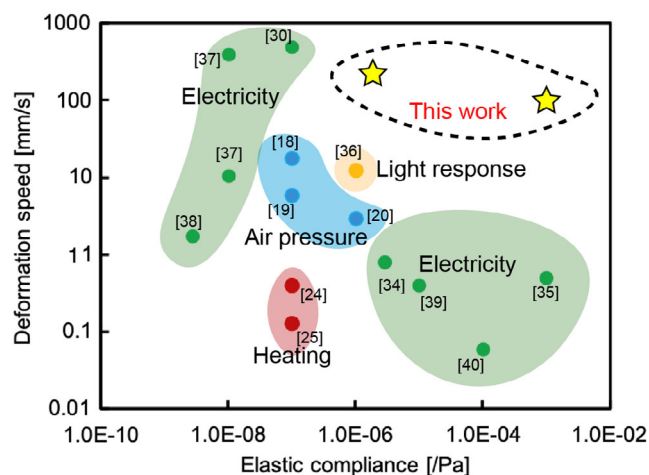


Figure 6. Comparison of elastic compliance and deformation speed with previous studies.

4. Conclusion

This study proposed a hydrogel actuator that achieves ultrafast drive and a large deformation using a Lorentz force. Gel fibers were wired inside an acrylamide gel, and an XY-axis stage that could move and rotate upon applying a current to different fibers was fabricated. Continuous trajectory control was realized by using a program to control the circuit. Vibration experiments using a coil-shaped gel fiber were conducted. An amplitude factor of 1.73 was achieved at a resonance frequency of 6 Hz (angular frequency: 37.7 rad s⁻¹), confirming the fast response of the system. A bending gripper using the fiber showed a deformation speed of 117.29 mm s⁻¹ (angular frequency: 5.24 rad s⁻¹). Finally, an electrically controlled ring gripper with a coil-shaped gel fiber achieved large deformation and could be used to transport gel pieces. Because the bending gripper can achieve ultrasoft contact, it can be applied in fields that require the handling of delicate objects such as human tissues, cells, and fragile foods

in the future. Further, because its expansion and contraction can be controlled, it can be applied to balloon catheters that are less damaging to blood vessels. The loss of water due to the heat dissipated by flow of current is a major problem for hydrogel actuators. However, when the actuator is used in water or any other liquid, as in this study, it reabsorbs water from the surrounding environment once the current is turned off, thus the actuator can be used repeatedly. We plan to investigate the improvement in the generative force by multiple connection, fabrication methods of the insulation coating, and the improvement in durability to expand the application of the proposed method in future work.

5. Experimental Section

Fabrication of Gel Fiber. The fabrication of gel springs with a core-shell structure was based on the microfluidic method according to the procedures established in the literature.^[26] Figure 1a shows the method for fabricating the gel fiber. Two types of gel fibers were fabricated: a straight shape (Figure 4a) and a coil shape (Figure 4b). Gel fibers with a core-shell structure were fabricated using microfluidic technology as follows. First, AlgNa was mixed into pure water. AlgNa(aq) was extruded from a microfluidic device consisting of coaxially aligned nozzles and a needle into the CaCl₂(aq) bath. A double nozzle was prepared using a 3D printer (AGIRISTA-3200, KEYENCE), and a syringe needle (NN-1838S, TERUMO) with an inner diameter of 0.82 μm was attached to the nozzle. To produce the core-shell structure, PVA aqueous solution (Arabic Yamato Standard, YAMATO Co., Ltd.) was injected from the inner part and AlgNa aqueous solution was injected from the outer part. The coil with a hydrogel having a core-shell structure was fabricated using microfluidic technology according to a previously reported procedure.^[43] An inclined nozzle was used to form a coil structure using the hydrogel. The inclination of the needle tip causes a difference in flow velocity between the interior and exterior of the needle. Therefore, there was an imbalance in the gel extrusion resulting in gel wrapping around the needle, creating a coil shape. The injection speed was adjusted to form straight- and coil-type liquid metal gel fibers, as shown in Figure 2. The injection speeds of PVA(aq) and AlgNa(aq) into 0.15 M CaCl₂(aq) were 0.06 and 0.20 mL min⁻¹, respectively. Young's modulus was measured by varying the density of AlgNa(aq) as 3%, 4%, 5%, and 6% (Figure S7, Supporting Information). The fabricated fibers were collected and assembled to fabricate three types of actuators: an XY-axis moving and rotating stage, a bending gripper, and a ring gripper. Liquid metal was injected into the core part by a syringe to replace PVA(aq) in the core part.

Fabrication Method of XY-Axis Moving and Rotating Stage: Figure S11a, Supporting Information, shows the fabrication process of the XY-axis moving and rotating stage. Two straight gel fibers were placed in a cross shape on a mold made of an acrylic plastic (Figure S11a(i), Supporting Information). Aqueous acrylamide comprising 25 mL of pure water, 2.2 g of acrylamide, 0.025 g of *N,N'*-methylenebis acrylamide (BIS), 60 μL of tetramethylethylenediamine (TEMED), and 0.01 g of ammonium persulfate (APS) in 25 mL of water was poured into the mold and sealed with a glass cover to prevent air from invading the hydrogel (Figure S11a(ii), Supporting Information). After 10 min, the gel stage was peeled off the mold.

Fabrication Method of Bending Gripper. Figure S11b, Supporting Information, shows the fabrication method of the bending gripper. One side of the bending gripper was fixed by a magnetic force to magnetic particles inside the hydrogel. As a result, the magnetic particles were embedded into one side of the gripper mold (Figure S11b(i), Supporting Information). Straight- and coil-shaped fibers were placed on an acrylic plate mold and inserted into the mold (Figure S11b(ii), Supporting Information). Then, a liquid gel composed of 25 mL of pure water, 2.2 g of acrylamide, 0.025 g of BIS, 60 μL of TEMED, and 0.01 g of APS was poured into the mold and cured. The cured gel gripper was peeled from the mold.

Fabrication Method of Ring Gripper: Figure S11c, Supporting Information, shows the fabrication method of the ring gripper. Only the handling part of the gripper needed to be cured. This part was fabricated using a photopolymerization method. An aqueous gel composed of pure water, acrylamide, BIS, and lithium phenyl(2,4,6-trimethylbenzoyl) phosphinate was filled in a plastic case, and the fabricated gel fiber was inserted into the bath. A photomask for curing the handling part of the gripper was placed on the case, and UV light was irradiated from the top for 1 min to complete the fabrication process.

Moving Method of Gel Actuator. Figure 1b shows the operation method of the gel actuator. When an electric current is passed through the gel fiber, a Lorentz force is generated by the magnetic force under the actuators. The Lorentz force is calculated as

$$F = I \cdot B \cdot L \quad (12)$$

Here, F is the Lorentz force; I is the current value; B is the magnetic flux density; and L is the fiber length. The direction of the force was determined by the directions of the current and the magnetic field. The actuator could be controlled in any direction by changing the amount and direction of current flow. The strength of the Lorentz force could be changed by varying the current and strength of the magnetic field. The theoretical value of the relationship between the moving or rotation speeds and the current in Figure 3c,g is described in Supporting texts 1 and 3 and Figure S1 and S3, Supporting Information.

Control of XY-Axis Moving Stage: The XY-axis moving stage was controlled by a circuit that could adjust the amount and direction of current flow (Figure S12, Supporting Information). Square orbit control of the device was performed by periodically changing the time and direction in which the current was passed through the two fibers. Figure S12, Supporting Information, shows the control method of the XY-axis moving stage. To control the stage in a square orbit, it is necessary to apply a reversible drive current to each gel fiber at arbitrary times and in arbitrary directions independently. For this purpose, a current drive circuit using metal-oxide-semiconductor field-emission transistor relays and a system that switches the relays using signals from an Arduino microcontroller were developed. Figure S12a, Supporting Information, shows the current drive circuit for one of the two fibers. When relays A1 and A2 were closed, Current A flowed in one direction. When relays B1 and B2 were closed, Current B flowed in the opposite direction. The switching time was determined by a computer. Figure S12b, Supporting Information, shows the output waveform of the microcontroller. The currents can be controlled by applying voltages to the relays. The same circuit was connected to another fiber. Therefore, the current can be applied to each fiber independently and reversibly.

Fiber Deformation Analysis using COMSOL: The Lorentz force and amount of deformation of the gel fiber by the force were calculated using COMSOL. The analyzed fiber had a diameter of 1 mm and Young's modulus of 0.79 MPa, which is the same as that of a gel fiber with an AlgNa concentration of 5%. In addition, the magnetic flux density of the neodymium magnet and ferrite magnet was 0.5 and 0.1 T, respectively. The dimensions were set to be the same as the actually measured parameters of the gel fiber. The amount of deformation was calculated by changing the current in the simulation.

Vibration of Gel Fiber. The coil-shaped gel fiber was vibrated using a function generator (AFG1062). A sine wave with a voltage of 5 V was applied to produce vibrations. Because this vibration system received a periodic external force, a forced vibration response occurred. The frequency response curve when a sine wave was applied was calculated from the equation of motion and compared with the experimental values.

Control of Grippers: Blue and red hydrogel-based objects were prepared to demonstrate transportation using a ring gripper. These objects were prepared by injecting liquid acrylamide into an acrylic mold fabricated by a cutting machine and then curing it. The objects were cylindrical, with a diameter of 10 mm and a height of 3 mm. The gripper was connected to the power supply with a copper wire. Two-color gels were placed from the desired left side to the desired upper right or lower right, respectively. The current at the time of expansion was set to 3.0 A.

Supporting Information

Supporting Information is available from the Wiley Online Library or from the author.

Acknowledgements

D.T. and K.M. equally contributed to this work. This work was supported by PRESTO/Japanese Science and Technology Agency (JST) (grant no. JPMJPR18J2), JST CREST Grant Number JP19209665, the Ogasawara research grant, and the SATOMI scholarship Foundation. H.O. acknowledges support from a Grant-in-Aid for Challenging Exploratory Research and Grant-in-Aid for Scientific Research (A) provided by the Japanese Society for the Promotion of Science.

Conflict of Interest

The authors declare no conflict of interest.

Data Availability Statement

Research data are not shared.

Keywords

electromagnetics, hydrogels, liquid metals, soft robots

Received: October 20, 2021

Revised: November 24, 2021

Published online:

- [1] R. L. Truby, M. Wehner, A. K. Grosskopf, D. M. Vogt, S. G. M. Uzel, R. J. Wood, J. A. Lewis, *Adv. Mater.* **2018**, *30*, 1.
- [2] Y. Gao, H. Ota, E. W. Schaler, K. Chen, A. Zhao, W. Gao, H. M. Fahad, Y. Leng, A. Zheng, F. Xiong, C. Zhang, L. C. Tai, P. Zhao, R. S. Fearing, A. Javey, *Adv. Mater.* **2017**, *29*, 1.
- [3] M. Bariya, H. Y. Y. Nyein, A. Javey, *Nat. Electron.* **2018**, *1*, 160.
- [4] Y. J. Tan, G. J. Susanto, H. P. Anwar Ali, B. C. K. Tee, *Adv. Mater.* **2020**, *2002800*, 1.
- [5] R. L. Truby, J. A. Lewis, *Nature* **2016**, *540*, 371.
- [6] Y. Morimoto, H. Onoe, S. Takeuchi, *Sci. Rob.* **2018**, *3*, 1.
- [7] Y. Yu, J. Nassar, C. Xu, J. Min, Y. Yang, A. Dai, R. Doshi, A. Huang, Y. Song, R. Gehlhar, A. D. Ames, W. Gao, *Sci. Rob.* **2020**, *5*, 1.
- [8] W. Gao, L. Wang, X. Wang, H. Liu, *ACS Appl. Mater. Interfaces* **2016**, *8*, 14182.
- [9] E. Palleau, D. Morales, M. D. Dickey, O. D. Velev, *Nat. Commun.* **2013**, *4*, 1.
- [10] D. Morales, I. Podolsky, R. W. Mailen, T. Shay, M. D. Dickey, O. D. Velev, *Micromachines* **2016**, *7*, 98.
- [11] S. Fujii, A. Nobukawa, T. Osaki, Y. Morimoto, K. Kamiya, N. Misawa, S. Takeuchi, *Lab Chip* **2017**, *17*, 2421.
- [12] W. W. Lee, Y. J. Tan, H. Yao, S. Li, H. H. See, M. Hon, K. A. Ng, B. Xiong, J. S. Ho, B. C. K. Tee, *Sci. Robot.* **2019**, *4*, eaax2198.
- [13] N. D. Shapiro, K. A. Mirica, S. Soh, S. T. Phillips, O. Taran, C. R. MacE, S. S. Shevkopylas, G. M. Whitesides, *J. Am. Chem. Soc.* **2012**, *134*, 5637.
- [14] A. P. McGuigan, D. A. Bruzewicz, A. Glavan, M. Butte, G. M. Whitesides, *PLoS One* **2008**, *3*, e2258.
- [15] Y. Li, G. Huang, M. Li, L. Wang, E. L. Elson, T. Jian Lu, G. M. Genin, F. Xu, *Sci. Rep.* **2016**, *6*, 1.
- [16] M. Wehner, R. L. Truby, D. J. Fitzgerald, B. Mosadegh, G. M. Whitesides, J. A. Lewis, R. J. Wood, *Nature* **2016**, *536*, 451.
- [17] E. J. Shin, W. H. Park, S. Y. Kim, *Appl. Sci.* **2018**, *8*, <https://doi.org/10.3390/app8081284>.
- [18] M. Schaffner, J. A. Faber, L. Pianegonda, P. A. Rühls, F. Coulter, A. R. Studart, *Nat. Commun.* **2018**, *9*, <https://doi.org/10.1038/s41467-018-03216-w>.
- [19] G. Agarwal, N. Besuchet, B. Audergon, J. Paik, *Sci. Rep.* **2016**, *6*, 1.
- [20] O. Azami, D. Morisaki, T. Miyazaki, T. Kanno, K. Kawashima, *Sens. Actuators, A Phys.* **2019**, *300*, 111623.
- [21] Acome, S. K. Mitchell, T. G. Morrissey, M. B. Emmett, C. Benjamin, M. King, M. Radakovitz, C. Keplinger, *Science* **2018**, *359*, 61.
- [22] J. Huang, S. Shian, Z. Suo, D. R. Clarke, *Adv. Funct. Mater.* **2013**, *23*, 5056.
- [23] S. J. A. Koh, C. Keplinger, T. Li, S. Bauer, Z. Suo, *IEEE/ASME Trans. Mechatron.* **2011**, *16*, 33.
- [24] A. Miriyev, K. Stack, H. Lipson, *Nat. Commun.* **2017**, *8*, 1.
- [25] A. Miriyev, G. Caires, H. Lipson, *Mater. Des.* **2018**, *145*, 232.
- [26] K. Matsubara, D. Tachibana, R. Matsuda, H. Onoe, O. Fuchiwaki, H. Ota, *Adv. Intell. Syst.* **2020**, *2*, 2000008.
- [27] H. Yuk, S. Lin, C. Ma, M. Takaffoli, N. X. Fang, X. Zhao, *Nat. Commun.* **2017**, *8*, <https://doi.org/10.1038/ncomms14230>.
- [28] T. Mitsumata, Y. Horikoshi, K. Negami, *Jpn. J. Appl. Phys.* **2008**, *47*, 7257.
- [29] M. Li, X. Wang, B. Dong, M. Sitti, *Nat. Commun.* **2020**, *11*, <https://doi.org/10.1038/s41467-020-17775-4>.
- [30] G. Mao, M. Drack, M. Karami-Mosammam, D. Wirthl, T. Stockinger, R. Schwödau, M. Kaltenbrunner, *Sci. Adv.* **2020**, *6*, eabc0251.
- [31] H. Shinoda, S. Azukizawa, K. Maeda, F. Tsumori, *J. Electrochem. Soc.* **2019**, *166*, B3235.
- [32] M. Lee, T. Park, C. Kim, S. M. Park, *Mater. Des.* **2020**, *195*, 108921.
- [33] S. Feng, X. Li, S. Wang, Z. Chen, *Electron. J. Geotech. Eng.* **2015**, *20*, 12113.
- [34] Y. Yan, T. Santaniello, L. G. Bettini, C. Minnai, A. Bellacicca, R. Porotti, I. Denti, G. Faraone, M. Merlini, C. Lenardi, P. Milani, *Adv. Mater.* **2017**, *29*, 1.
- [35] G. Haghiashtiani, E. Habtour, S. H. Park, F. Gardea, M. C. McAlpine, *Extrem. Mech. Lett.* **2018**, *21*, 1.
- [36] M. Pilz da Cunha, Y. Foelen, R. J. H. van Raak, J. N. Murphy, T. A. P. Engels, M. G. Debije, A. P. H. J. Schenning, *Adv. Opt. Mater.* **2019**, *7*, 1801643.
- [37] O. Kim, S. J. Kim, M. J. Park, *Chem. Commun.* **2018**, *54*, 4895.
- [38] K. Song, S. H. Kim, S. Jin, S. Kim, S. Lee, J. S. Kim, J. M. Park, Y. Cha, *Sci. Rep.* **2019**, *9*, 1.
- [39] C. Shen, Q. Zhao, C. M. Evans, *Adv. Mater. Technol.* **2019**, *4*, 1.
- [40] C. Yuan, D. J. Roach, C. K. Dunn, Q. Mu, X. Kuang, C. M. Yakacki, T. J. Wang, K. Yu, H. J. Qi, *Soft Matter* **2017**, *13*, 5558.
- [41] Y. Li, Y. Li, M. Hashimoto, *Sens. Actuators, B Chem.* **2019**, *282*, 482.
- [42] J. Guo, C. Xiang, T. Helps, M. Taghavi, J. Rossiter, *2018 IEEE Int. Conf. Soft Robot. RoboSoft*, IEEE, Piscataway, NJ **2018**, p. 339.
- [43] K. Yoshida, H. Onoe, *Sci. Rep.* **2017**, *7*, 1.

Supporting Information

Title

Ultrafast and Highly Deformable Electromagnetic Hydrogel Actuators Assembled from Liquid Metal Gel Fiber

Author(s), and Corresponding Author(s)*

D. Tachibana¹, K. Murakami¹, T. Kozaki¹, R. Matsuda¹, Y. Isoda², F. Nakamura¹, Y. Isano¹, K. Ueno³, O. Fuchiwaki^{1,2*}, H. Ota^{1,2*}

Supporting text 1. Theory of movement of moving stages.

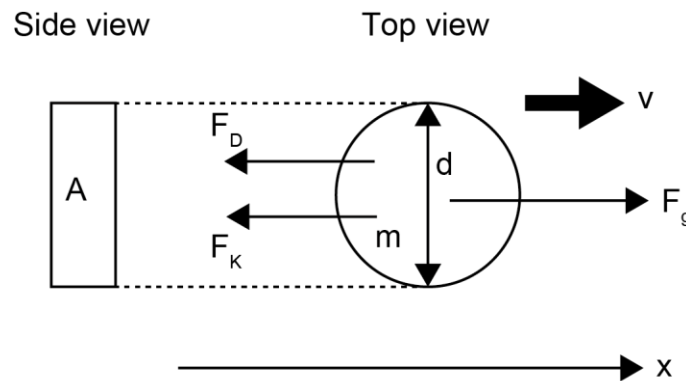


Fig. S1. Mechanical model of XY-axis moving stage.

Figure S1 shows the mechanical model of the XY-axis moving stage. The parameters are defined as follows:

m : weight of stage

v : velocity of stage

d : diameter of stage

A : projected area of stage along movement direction

F_g : Lorentz force

B : magnetic flux density

I : current

L : length of wire fixed to stage (in oblique case, projection onto plane perpendicular to velocity vector)

F_D : drag force acting on stage from surrounding fluid (water)

μ : viscosity coefficient of fluid

ρ : density of fluid

F_k : damping terms due to changes in tension and magnetic flux density

C_D : drag coefficient

Re : Reynolds number

Based on Figure S1, the equation of motion is

$$m\ddot{x} = F_g - F_D - F_k \quad (13)$$

Here, the force acting on the moving stage is defined as

$$F_g = BIL \quad (14)$$

$$F_D = C_D A \cdot \frac{1}{2} \rho v^2 \quad (15)$$

$$F_k = kx \quad (16)$$

The moving stage is under tension from the copper wire. Further, the strength of the magnetic field weakens as it moves away from the center of the magnet. Therefore, the damping force is defined as $F_k = kx$.

Because the drag coefficient is $1 < Re < 10^4$, it is obtained as [1]

$$C_D = \left(0.55 + \frac{4.8}{\sqrt{Re}}\right)^2 \quad (17)$$

From the above, the equation of motion can be transformed as

$$m\ddot{x} = BIL - C_D A \cdot \frac{1}{2} \rho v^2 - kx \quad (18)$$

$$\ddot{x} = \frac{BIL}{m} - \frac{C_D A}{m} \cdot \frac{1}{2} \rho v^2 - \frac{k}{m} x$$

$$\ddot{x} + ax^2 + bx = c \quad (19)$$

Based on Eq. (19), the parameters a, b, and c can be obtained as follows:

$$a = \frac{C_D A}{m} \cdot \frac{1}{2} \rho \quad (20)$$

$$b = \frac{k}{m} \quad (21)$$

$$c = \frac{BIL}{m} \quad (22)$$

Here, x is assumed to be monotonic with respect to time t . x and t are assumed to be in one-to-one correspondence. x is treated as an independent variable.

$$\ddot{x} = \frac{d}{dt} \dot{x} = \frac{d}{dt} v(x) = \frac{dx}{dt} \cdot \frac{dv(x)}{dx} = v(x) \cdot \frac{dv(x)}{dx} \quad (23)$$

Here, $\frac{dx}{dt}$ is defined as

$$\frac{dx}{dt} = v(x) \quad (24)$$

Eq. (24) gives

$$v(x) \cdot \frac{dv(x)}{dx} + av(x)^2 = -bx + c \quad (25)$$

Further, $u(x)$ is assumed as

$$u(x) = v(x)^2 \quad (26)$$

$$\frac{du(x)}{dx} = 2v(x) \frac{dv(x)}{dx} \quad (27)$$

The equations of motion can be altered as

$$\frac{du(x)}{dx} + 2au(x) = -2bx + 2c \quad (28)$$

Here, $\mu(x)$ is assumed as

$$\mu(x) = e^{\int 2adx} = e^{2ax} \quad (29)$$

From Eq. (29), the following equations of motion can be obtained:

$$e^{2ax} \cdot \frac{du(x)}{dx} + 2ae^{2ax} \cdot u(x) = e^{2ax}(-2bx + 2c) \quad (30)$$

$$e^{2ax} \cdot \frac{du(x)}{dx} + \frac{d}{dx} e^{2ax} \cdot u(x) = e^{2ax}(-2bx + 2c) \quad (31)$$

$$\frac{d}{dx} \{e^{2ax} \cdot u(x)\} = e^{2ax}(-2bx + 2c) \quad (32)$$

$$\int \frac{d}{dx} \{e^{2ax} \cdot u(x)\} dx = \int e^{2ax}(-2bx + 2c) dx \quad (33)$$

$$e^{2ax} \cdot u(x) = e^{2ax} \left(-\frac{b}{a}x + \frac{c}{a} + \frac{b}{2a^2} \right) + C \quad (34)$$

$$u(x) = -\frac{b}{a}x + \frac{c}{a} + \frac{b}{2a^2} + Ce^{-2ax} \quad (35)$$

x is assumed as

$$-\frac{b}{a}x + \frac{c}{a} + \frac{b}{2a^2} + Ce^{-2ax} > 0$$

$u(x)$ can be assumed as

$$u(x) = v(x)^2$$

$$v(x) = \pm \sqrt{-\frac{b}{a}x + \frac{c}{a} + \frac{b}{2a^2} + Ce^{-2ax}} \quad (36)$$

x is defined as

$$-\frac{b}{a}x + \frac{c}{a} + \frac{b}{2a^2} + Ce^{-2ax} > 0$$

The initial conditions of $v(t)$ and $x(t)$ can be defined as

$$\begin{aligned} v(t)|_{t=0} &= v(0) = 0 \\ x(t)|_{t=0} &= x(0) = 0 \end{aligned} \quad (37)$$

Therefore, $v(x)$ is given as

$$v(x)|_{x=0} = v(0) = 0$$

$$v(0) = 0 = \pm \sqrt{\frac{c}{a} + \frac{b}{2a^2} + C} \quad (38)$$

$$C = -\left(\frac{c}{a} + \frac{b}{2a^2}\right) \quad (39)$$

$$v(x) = \pm \sqrt{-\frac{b}{a}x + \left(\frac{c}{a} + \frac{b}{2a^2}\right)(1 - e^{-2ax})} \quad (40)$$

x can be assumed as

$$-\frac{b}{a}x + \left(\frac{c}{a} + \frac{b}{2a^2}\right)(1 - e^{-2ax}) > 0$$

$$v(t) = \frac{dx(t)}{dt} = \pm \sqrt{-\frac{b}{a}x + \left(\frac{c}{a} + \frac{b}{2a^2}\right)(1 - e^{-2ax})} \quad (41)$$

x can be assumed as

$$-\frac{b}{a}x + \left(\frac{c}{a} + \frac{b}{2a^2}\right)(1 - e^{-2ax}) > 0$$

$$\int_{x(0)}^{x(t)} \frac{dx(t)}{\pm \sqrt{-\frac{b}{a}x + \left(\frac{c}{a} + \frac{b}{2a^2}\right)(1 - e^{-2ax})}} = \int_0^t dt \quad (42)$$

$$\int_0^{x(t)} \frac{dx(t)}{\pm \sqrt{-\frac{b}{a}x + \left(\frac{c}{a} + \frac{b}{2a^2}\right)(1 - e^{-2ax})}} = t \quad (43)$$

To find $x(t)$, Eq. (43) needs to be solved, which involves integration.

Her, an approximate solution to $x(t)$ is found through numerical calculations using Wolfram Alpha with the fourth-order Runge-Kutta method.

[1] Allen, T. 1981, *Particle Size Measurement*, Chapman & Hall, 3rd edition.

Supporting text 2. Theory of angle calculation of XY-axis moving stage.

The movement direction of the XY-axis moving stage was determined by the vector sum of the Lorentz forces generated along the two axes. The current values of the fibers along the X- and Y-axes were defined as I_X and I_Y , respectively. The angle of movement from the X-axis changed according to the ratio $I_X:I_Y$, as shown in Table S1. Figure S2 shows the method for calculating the angle. When the magnetic flux density is B and the fiber length is L , Lorentz forces of I_YBL and I_XBL are generated along the X- and Y-axes, respectively. By combining the two Lorentz force vectors, the angle θ from the X-axis in the movement direction is calculated as

$$\theta = \tan^{-1} \frac{I_X BL}{I_Y BL} = \tan^{-1} \frac{I_X}{I_Y} \quad (44)$$

Table S1. Current ratio and angle from X-axis.

$I_X:I_Y$	0:1	1:2	1:1	2:1	1:0
Theoretical angle from x-axis: θ [°]	0	26.6	45	63.4	90

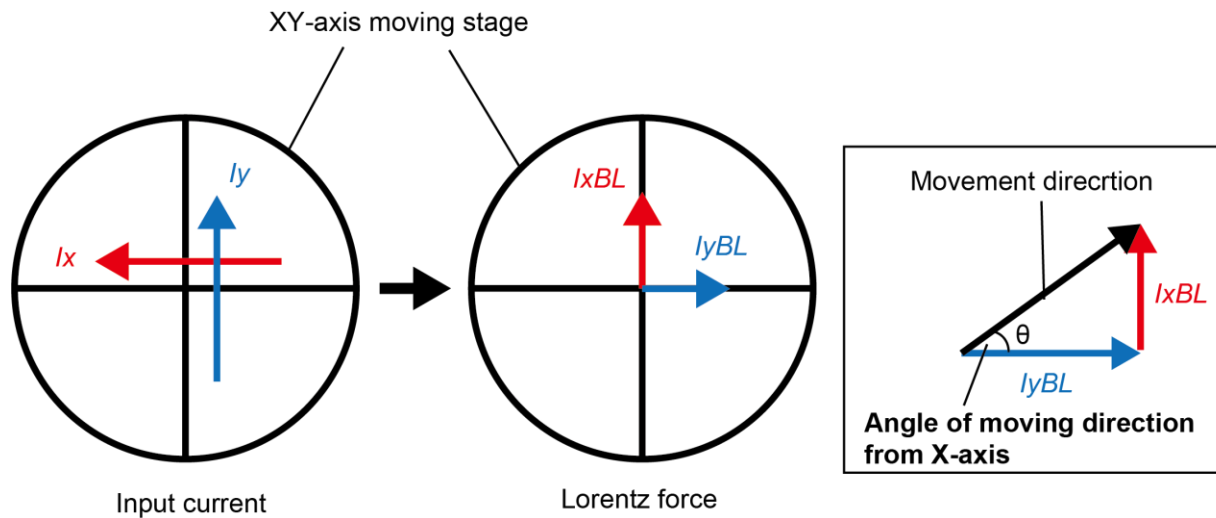


Figure S2. Calculation method of movement direction of XY-axis moving stage. Two Lorentz forces I_YBL and I_XBL are generated along the X- and Y-axes, respectively, when currents I_X and I_Y are input along the X- and Y-axes, respectively. The two Lorentz force vectors are combined to calculate the angle of the moving direction from the X-axis.

Supporting text 3. Theory of rotation of moving stages

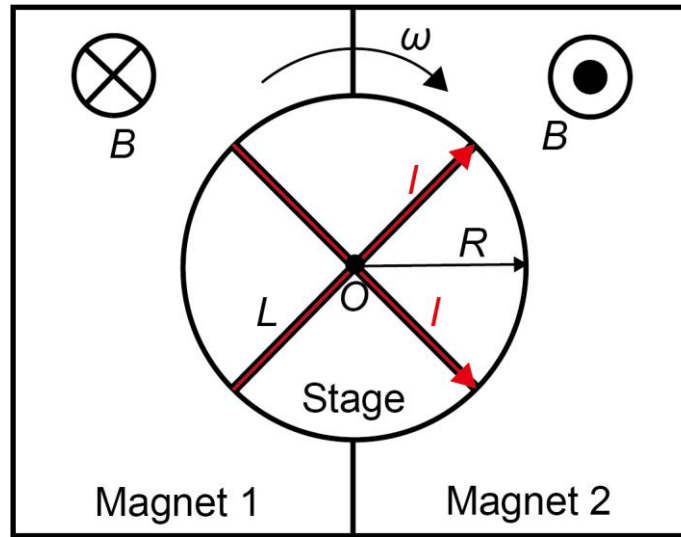


Figure S3. Mechanical model of rotation of moving stage from top view

Figure S3 shows the mechanical model of the rotation of the moving stage. The parameters are defined as follows:

J : moment of inertia

ω : angular velocity of stage

V : velocity of stage

R : radius of stage

L : length of gel fiber

$\Delta F_g(r)$: Lorentz force acting on wire ΔL

N_g : torque due to Lorentz force (moment of force)

B : magnetic flux density (constant)

I : current (constant)

$\Delta F_d(r)$: viscous force acting from fluid on circular ring of radius r to $r + \Delta r$ of stage

η : viscosity coefficient of fluid (air)

F_k : tension of wiring (for one wire)

N_k : torque due to tension of wiring (for four wires)

The equation of motion for rotation is as follows. The resistance torque due to the tension of the wires is negligible and is assumed to be zero.

$$J\ddot{\theta} = N_g - N_D - N_k \quad (45)$$

The Lorentz force acting on the wiring Δl is

$$\Delta F_g(r) = BI\Delta l \quad (46)$$

The sum of the resistive torques due to the Lorentz force acting on the wiring Δl of the stage can be expressed as

$$N_g = 4 \int_0^R BILdL = 2BIR^2 \quad (47)$$

The velocity at the position of the radius r of the stage is

$$V(r) = r\dot{\theta} \quad (48)$$

The viscous force acting on a circular ring of radius r to $r + \Delta r$ of the stage is

$$\Delta F_d(r) = \eta \frac{V(r)}{h} (2\pi r \Delta r) \quad (49)$$

Substituting Eq. (41) into Eq. (42) gives the viscous force acting on the circular ring of radius r to $r + \Delta r$ of the stage as

$$\Delta F_d(r) = 2\pi \frac{\eta \dot{\theta}}{h} r^2 \Delta r \quad (50)$$

As a result, the total viscous torque due to the viscous force of the entire stage is

$$N_D = \int_0^R r \cdot \Delta F_d(r) = 2\pi \frac{\eta}{h} \dot{\theta} \int_0^R r^3 \Delta r = \frac{1}{2} \pi \frac{\eta}{h} R^4 \dot{\theta} \quad (51)$$

The wiring tension F_k in each wire is defined as

$$F_k = k\theta \quad (52)$$

The total viscous torque due to the viscous force of the entire stage is

$$N_k = 2F_k \cdot 2R = 4k\theta R \quad (53)$$

From $\omega = \dot{\theta}$, Eqs. (47) and (53) are substituted into Eq. (45). The equation of motion for rotation is

$$J\ddot{\theta} = 2BIR^2 - \frac{1}{2} \pi \frac{\eta}{h} R^4 \dot{\theta} - 4k\theta R \quad (54)$$

The viscous force of air, $-\frac{1}{2}\pi\frac{\eta}{h}R^4\dot{\theta}$, is negligible because it is relatively small and is approximated to be zero.

The equation of motion for rotation can be simplified as

$$\ddot{\theta} + a\theta = b \quad (55)$$

In this equation, a and b are defined as

$$a \equiv \frac{4kR}{J} \quad (56)$$

$$b \equiv \frac{2BIR^2}{J} \quad (57)$$

θ_0 in the homogeneous equation $\ddot{\theta} + a\theta = 0$ is

$$\theta_0 = A\sin\sqrt{a}t + B\cos\sqrt{a}t \quad (58)$$

The special solution θ_1 and general solutions θ are defined as

$$\theta_1 = \frac{b}{a} = \frac{BIR}{2k} \quad (59)$$

$$\theta = A\sin\sqrt{a}t + B\cos\sqrt{a}t + \frac{b}{a} \quad (60)$$

θ is derived by defining the initial conditions as

$$\theta(0) = \dot{\theta}(0) = 0 \quad (61)$$

$\theta(0) = 0$ gives

$$\begin{aligned} \theta = 0 &= B + \frac{b}{a} \\ B &= -\frac{b}{a} \end{aligned} \quad (62)$$

Differentiating θ gives

$$\begin{aligned} \dot{\theta}(t) &= \sqrt{a}(A\cos\sqrt{a}t - B\sin\sqrt{a}t) \\ \dot{\theta}(0) = 0 &= A\sqrt{a} \\ A &= 0 \end{aligned} \quad (63)$$

The angle θ and angular velocity $\dot{\theta}$ are defined as

$$\theta = \frac{b}{a}(-\cos\sqrt{at} + 1) \quad (64)$$

$$\dot{\theta} = \frac{b}{\sqrt{a}}\sin\sqrt{at} \quad (65)$$

$$\frac{b}{a} = \frac{BIR}{2k} \quad (66)$$

$$\sqrt{a} = \sqrt{\frac{4kR}{J}}$$

The moment of inertia J of the disk is

$$J = \frac{1}{2}mR^2 \quad (67)$$

$$J = \int_0^R r^2 \cdot \rho 2\pi r \cdot d_c dr = 2\pi\rho d_c \frac{R^4}{4} = \frac{1}{2}mR^2$$

From the above, Eq. (65) becomes

$$\dot{\theta} = \frac{BIR}{2k} \left(-\cos 2\sqrt{\frac{2k}{mR}}t + 1\right) \quad (68)$$

The rotation angle at each elapsed time was calculated by substituting Eq. (68).

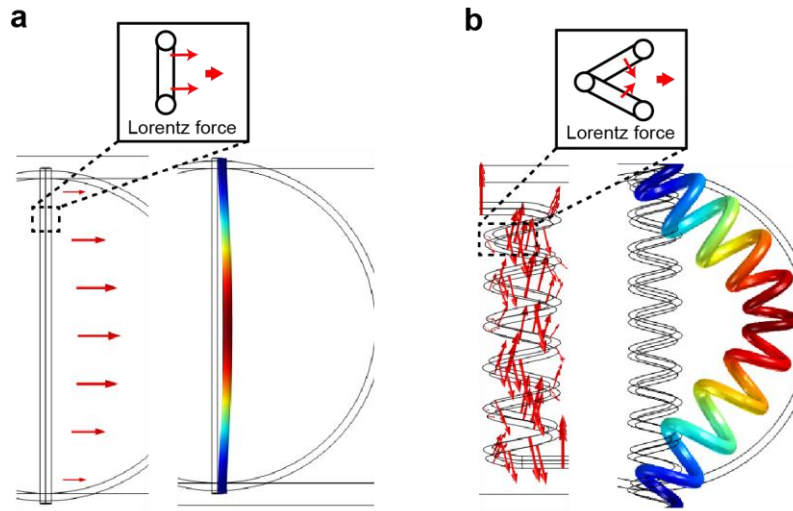


Figure S4. Simulation images of Lorentz force vectors in straight- and coil-type fibers as obtained using COMSOL. a. Deformation of a straight-type gel fiber with a current of 2.0 A. The Lorentz force is generated in one direction. b. Deformation of a coil-type gel fiber with a current of 2.0 A. The Lorentz force is generated in various directions. However the direction is the same as that of the straight-type gel fiber when the vectors are combined.

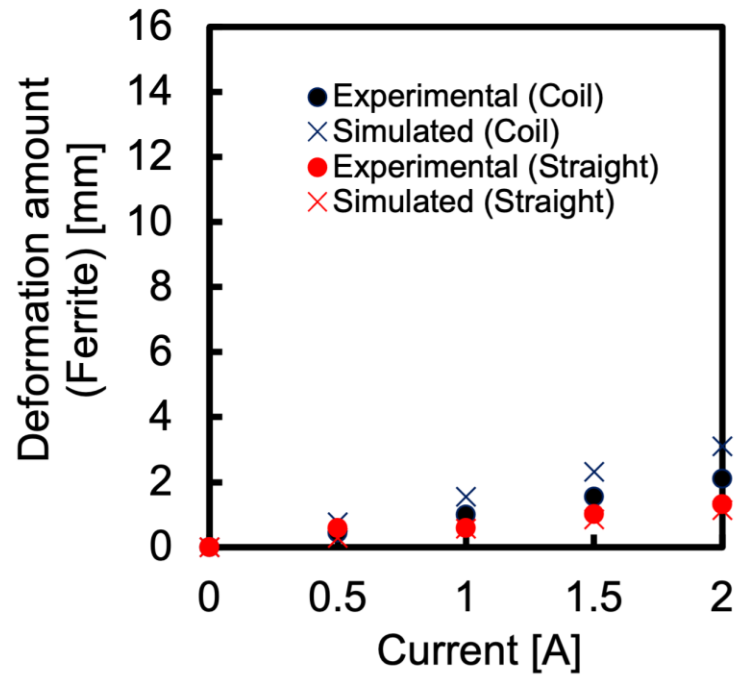


Figure S5. Relationship between current and amount of deformation of gel fiber using ferrite magnet. The amount of deformation increased with the current. The amount of deformation of the coil-type fiber was larger than that of the straight-type fiber. The amount of deformation with ferrite magnets was smaller than that with neodymium magnets owing to the smaller magnetic force.

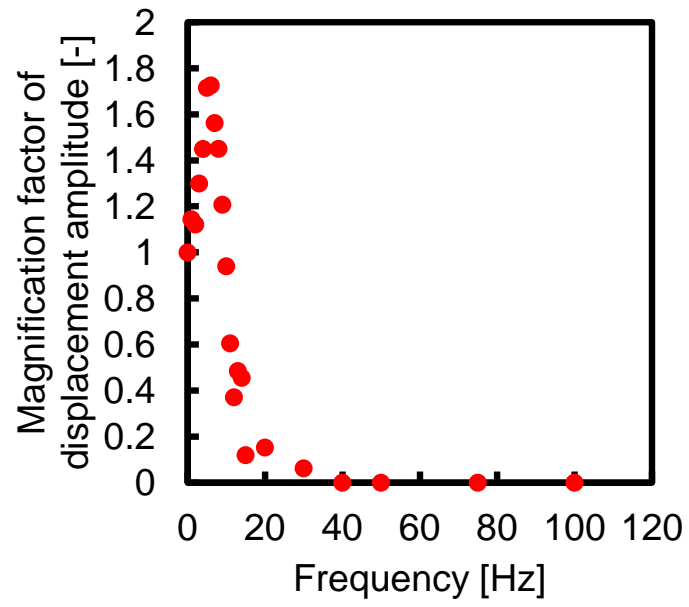


Figure S6. Relationship between Magnification factor of displacement amplitude and frequency.

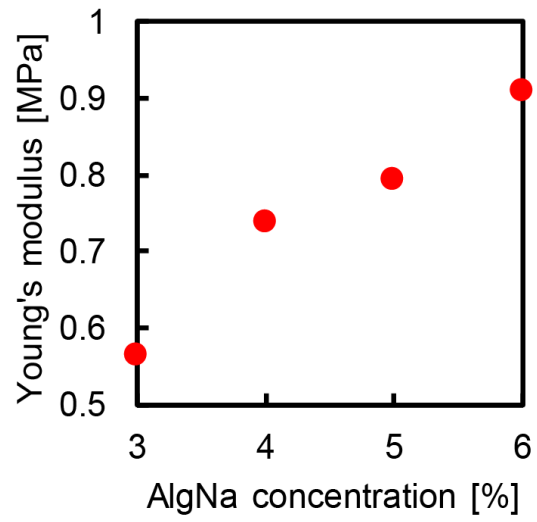


Figure S7. Relationship between AlgNa concentration and Young's modulus of gel fiber. Young's modulus of the gel fiber increased as a function of the AlgNa concentration.

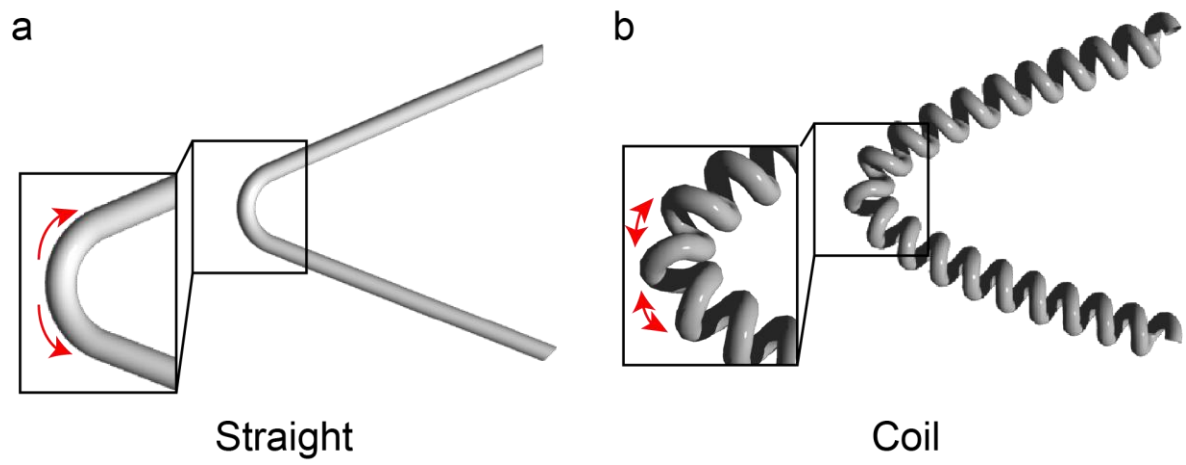


Figure S8. Difference in bending method between straight-shaped fiber and coil-shaped fiber. a. In the straight-type fiber, bending deformation is caused by the expansion of the fiber. b. In the coil-type fiber, bending deformation is caused by changes in the pitch of the coil.

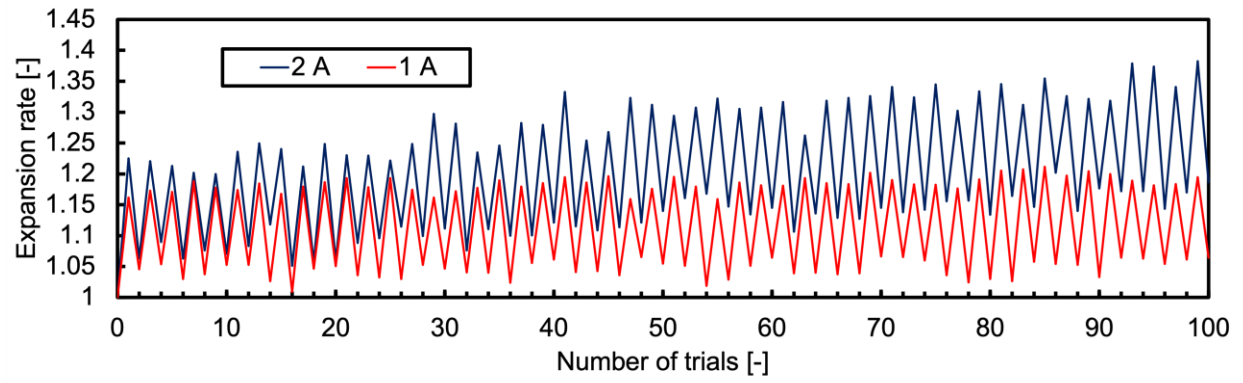


Figure S9. Repeatability test of a ring gripper at currents of 1 and 2 A.

Supporting text 4. Vibration theory of gel fiber using a mechanical model.

The vibration of the coil-type gel fiber, as shown in Figure 4e, is described theoretically when the actuator was modelled by a second order lag element, as follows:

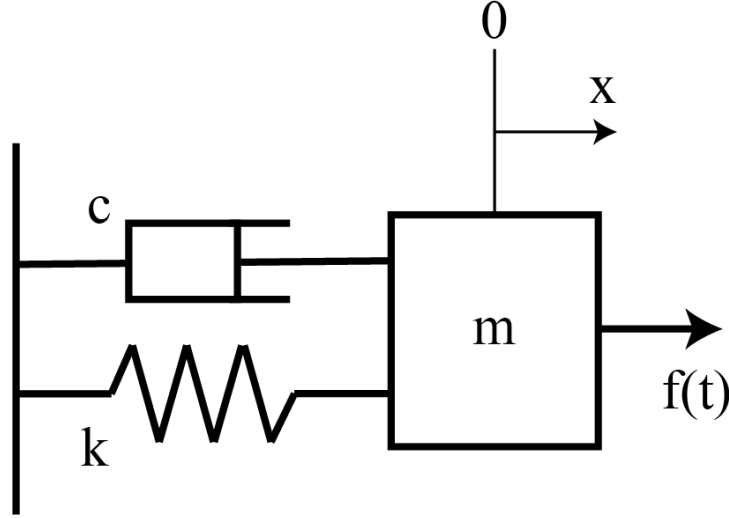


Figure S10. Vibration model.

As shown in Figure S10, a vibrating system with a spring and a damper attached to an object of mass m is assumed. The spring has a restoring force with spring constant k , and the damper has a damping force proportional to the velocity (damping coefficient: c). The displacement under a dynamic external force is $x(t)$, and the external force acting on the object is $f(t)$. The equation of motion is

$$m\ddot{x} + c\dot{x} + kx = f(t) \quad (69)$$

To obtain the vibration response when a cyclic external force acts on a one-degree-of-freedom vibration system, the cyclic force is assumed as

$$f(t) = f_0 \cos \omega t \quad (70)$$

f_0 and ω are the amplitude and angular frequency of the periodic force, respectively, and t is the time.

Substituting the above equation into Eq. (62) gives the following differential equation:

$$m\ddot{x} + c\dot{x} + kx = f_0 \cos \omega t \quad (71)$$

$$\omega_n = \sqrt{\frac{k}{m}} \quad (72)$$
$$\zeta = \frac{c}{c_c}$$

$$c_c = 2\sqrt{mk}$$

$$x_s = \frac{f_0}{k}$$

Using Eq. (72) and reformulating Eq. (71) gives

$$\ddot{x} + 2\zeta\omega_n\dot{x} + \omega_n^2x = x_s\omega_n^2\cos\omega t \quad (73)$$

where x_s represents the corresponding static displacement when an external force of $x_s\omega_n^2$ acts statically. Here, the steady-state response of Eq. (66) is calculated. Because the periodic external force term includes $\cos\omega t$, it is predicted that $\cos\omega t$ synchronized with the excitation force will also be part of the solution. In addition, the differential equation includes the first-order derivative of x . Therefore, in addition to $\cos\omega t$, $\sin\omega t$ must also be part of the solution. The solution of the equation is

$$x = C\cos\omega t + S\sin\omega t \quad (74)$$

Here, C and S are unknowns. Transforming Eq. (67) gives

$$x = A\cos(\omega t - \varphi) \quad (75)$$

Here, A is the amplitude and φ is the phase angle. A comparison of Eq. (75) with Eq. (74) gives $C = A\cos\varphi$ and $S = A\sin\varphi$. This, in turn, gives

$$A = \sqrt{C^2 + S^2} \quad (76)$$

$$\varphi = \sin^{-1}(S/A) = \cos^{-1}(C/A) = \tan^{-1}(S/C)$$

Eq. (74) is substituted into Eq. (73). Then, by comparing the vibration components for each term of $\cos\omega t$ and $\sin\omega t$, the following equations for C and S are obtained:

$$\left\{1 - \left(\frac{\omega}{\omega_n}\right)^2\right\}C + 2\zeta\left(\frac{\omega}{\omega_n}\right)S = x_s \quad (77)$$

$$-2\zeta\left(\frac{\omega}{\omega_n}\right)C + \left\{1 - \left(\frac{\omega}{\omega_n}\right)^2\right\}S = 0$$

By calculating the above equation and substituting C and S into Eq. (74), the steady-state response under a forced vibration is obtained as

$$x = \frac{x_s}{\left\{1 - \left(\frac{\omega}{\omega_n}\right)^2\right\}^2 + \left(2\zeta\frac{\omega}{\omega_n}\right)^2} \left[\left\{1 - \left(\frac{\omega}{\omega_n}\right)^2\right\} \cos\omega t + 2\zeta\frac{\omega}{\omega_n} \sin\omega t \right] \quad (78)$$

In a vibrating system subjected to periodic external forces, a forced vibration response is generated. Recalculating the oscillatory solution in Eq. (82) into the expression in Eq. (79) gives

$$x = M_d x_s \cos(\omega t - \varphi) = x_d \cos(\omega t - \varphi) \quad (79)$$

In Eq. (79), M_d is

$$M_d = \frac{1}{\sqrt{\left\{1 - \left(\frac{\omega}{\omega_n}\right)^2\right\}^2 + \left(2\zeta \frac{\omega}{\omega_n}\right)^2}} \quad (80)$$
$$= \frac{x_d}{x_s}$$

M_d is the ratio of the response amplitude x_d to the static deformation x_s , which is called the magnification factor of the displacement amplitude. This magnification factor was used as the theoretical value and compared with the experimental value while varying ζ . The resonance frequency obtained from the experiment was substituted for ω_n . Figure 4e is obtained by varying the frequency of $2\pi\omega$ from 0 to 100 Hz.

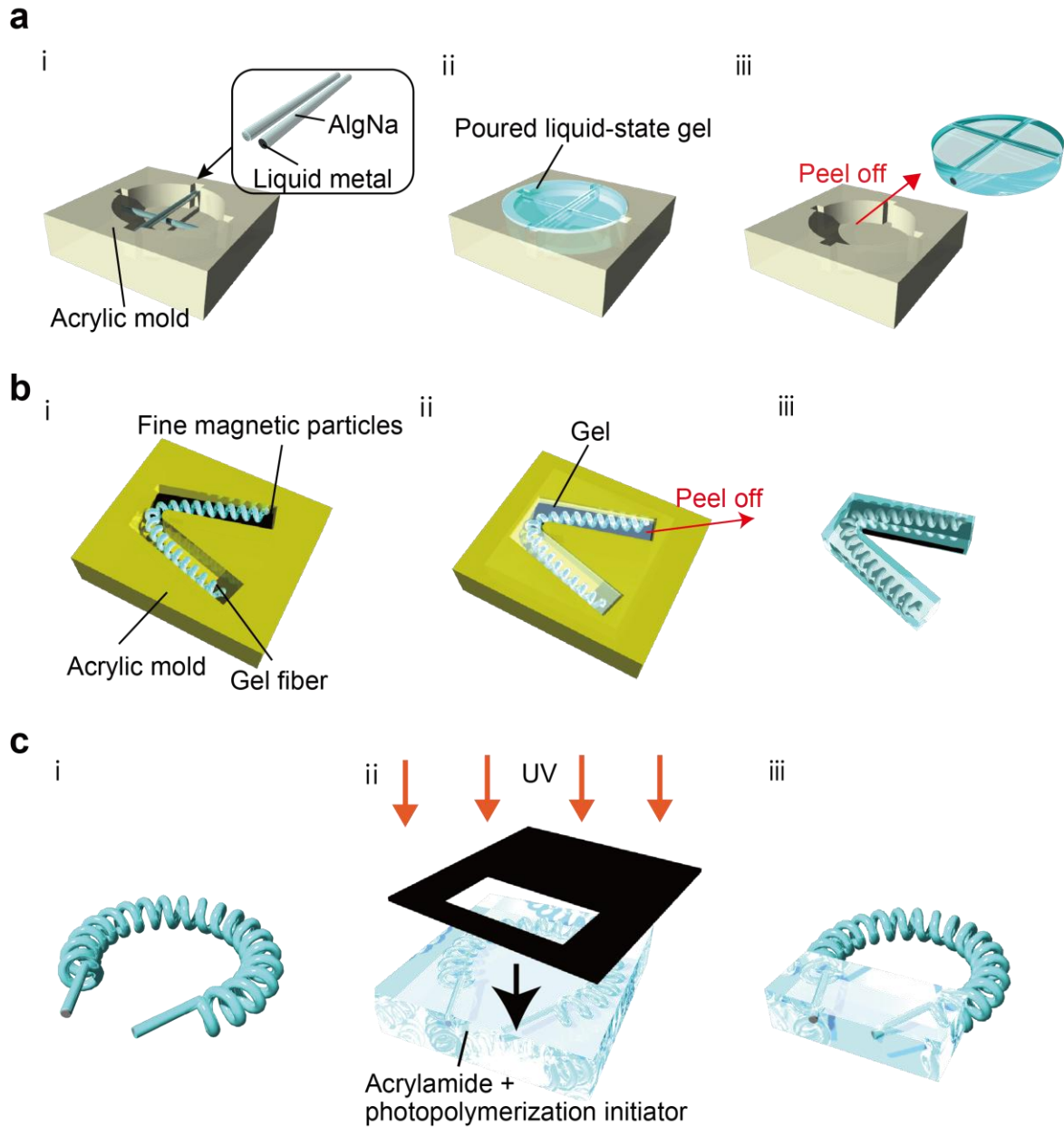


Figure S11. Fabrication methods of gel actuator. a. Fabrication method of XY-axis moving stage. Two gel fibers were placed on top of a mold cut from an acrylic sheet, and liquid gel was poured into the fibers (i). After the gel had cured (ii), it was peeled off from the mold (iii). b. Fabrication method of bending gripper. The gel fibers were placed on top of a mold and magnetic particles were inserted in one side of the mold (i). The liquid gel was poured into the mold, and after the gel cured (ii), it was peeled off from the mold (iii). c. Fabrication method of ring gripper. A liquid gel containing a photopolymerization curing agent was filled in a container, and a ring-shaped gel fiber was placed in the container (i). A photomask was prepared, and visible light was irradiated from above to cure a portion of the gel (ii–iii).

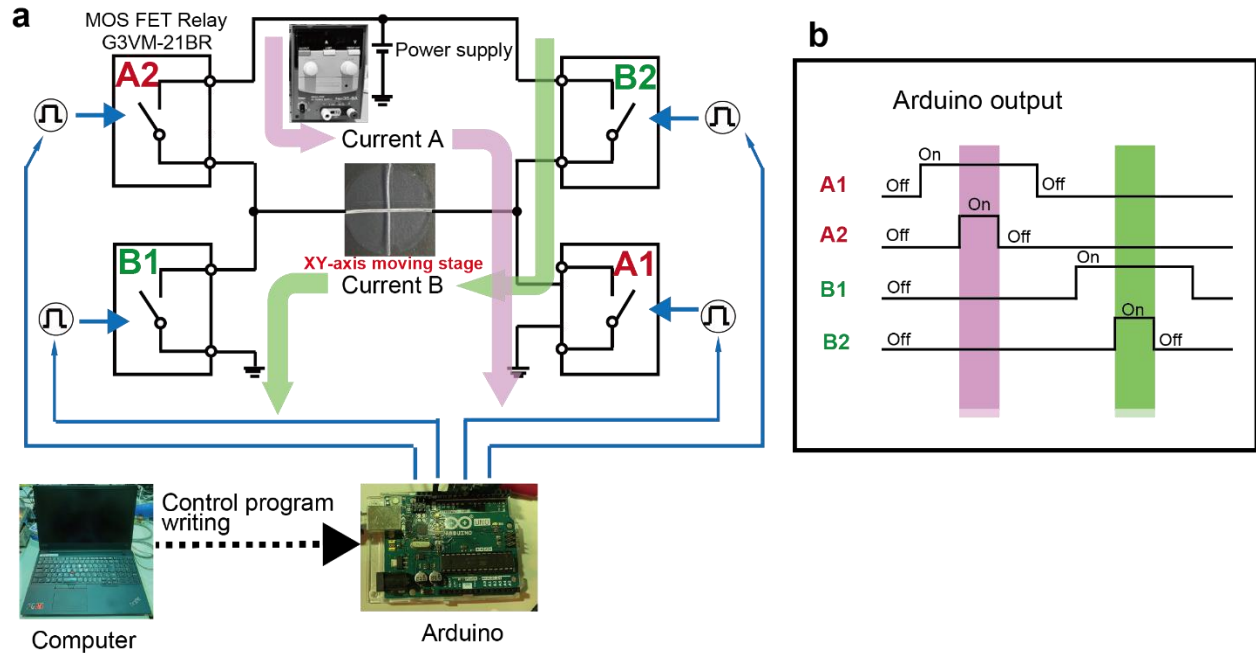


Figure S12. Circuit and system to control XY-axis moving stage. a. Circuit diagram of connecting to gel fiber. Current A flows in one direction when relays A1 and A2 are closed. By contrast, Current B flows in the opposite direction when relays B1 and B2 are closed. This system enables a reversible current flow to the fiber. A computer program was written in the Arduino microcontroller to switch the relays at any desired time. b. Output waveform of Arduino microcontroller. The output time and timing can be adjusted using this microcontroller.

Movie S1. Demonstration of liquids mixing using vibration of gel fibers.

Movie S2. Movement of bending gripper.

Movie S3. Movement of ring gripper.

Movie S4. Demonstration of ring gripper capturing and releasing a gel.